Flt-1 Signaling in Macrophages Promotes Glioma Growth *In vivo*

Mark Kerber,[1] Yvonne Reiss,[2] Anke Wickersheim,[1] Manfred Jugold,[3] Fabian Kiessling,[3] Matthias Heil,[4] Vadim Tchaikovski,[5] Johannes Waltenberger,[5] Masabumi Shibuya,[6] Karl H. Plate,[2] and Marcia Regina Machein[1]

[1]Tumor Angiogenesis Research Group, Department of Neurosurgery, University of Freiburg, Freiburg, Germany; [2]Institute of Neurology, Edinger Institute, University of Frankfurt, Frankfurt, Germany; [3]Department of Medical Physics in Radiology, Junior Group Molecular Imaging, German Cancer Research Center, Heidelberg, Germany; [4]Department of Experimental Cardiology, Max-Planck Institute for Heart and Lung Research, Bad Nauheim, Germany; [5]Department of Cardiology and Cardiovascular Research Institute Maastricht, Maastricht, the Netherlands; and [6]Department of Genetics, Institute of Medical Science, University of Tokyo, Tokyo, Japan

Abstract

Several lines of evidence indicate that Flt-1, a fms-like tyrosine kinase receptor, which binds to vascular endothelial growth factor (VEGF)-A, VEGF-B, and PlGF, is a positive regulator of angiogenesis in the context of tumor growth and metastasis. However, the molecular basis of its action is still not clear. Besides endothelial cells, Flt-1 is also expressed by other different cell types, including myeloid hematopoeitic cells (monocytes and macrophages). To examine the functions of Flt-1 expressed by bone marrow–derived myeloid cells in supporting tumor growth and angiogenesis, Flt-1 tyrosine kinase–deficient (Flt-1 TK−/−) bone marrow cells were transplanted into lethally irradiated syngeneic recipients. After hematopoietic reconstitution, we orthotopically implanted syngeneic wild-type glioma cells or glioma cells overexpressing either $VEGF_{164}$ or PlGF-2. Loss of Flt-1 signaling in bone marrow–derived myeloid cells led to a significant decrease in tumor volume and vascularization in gliomas. VEGF but not PlGF overexpressed by glioma cells restored the tumor growth rate in Flt-1 TK−/− bone marrow chimera. VEGF and PlGF overexpression by tumor cells induced an accumulation of bone marrow–derived myeloid cells into tumor tissue. This infiltration was decreased in tumors grown in Flt-1 TK−/− bone marrow chimeras. When investigating chemokines and growth factors involved in myeloid cell recruitment, we determined elevated SDF-1/CXCL12 levels in VEGF- and PlGF-overexpressing tumors. Collectively, these results suggest that Flt-1 signaling in myeloid cells is essential to amplify the angiogenic response and to promote glioma growth. [Cancer Res 2008;68(18):7342–51]

Introduction

Vascular endothelial growth factor (VEGF) is an essential angiogenic growth factor to provide sufficient blood supply in tumors. The VEGF family is composed of five structurally related molecules: PlGF, VEGF-A, VEGF-B, VEGF-C, and VEGF-D (1). The biological function of VEGF family members is mediated by the activation of tyrosine kinase receptors structurally related to fms/kit/PDGFR family. VEGFRs (VEGFR-1/flt-1, VEGFR-2/flk-2, and VEGFR-3/flt-4) are characterized by an extracellular binding domain carrying seven immunoglobulin-like sequences and a cytoplasmic tyrosine kinase domain (2). The specific binding pattern of VEGF family ligands to the receptors modulated different activities. Flk-1 in response to VEGF mediates the angiogenic signals and vascular permeability in blood vessels (3), whereas Flt-4, which interacts with VEGF-D and VEGF-C, transduces signals relevant for lymphatic vessel growth (4).

Until now, the function of Flt-1 is still not completely understood. VEGF-A, VEGF-B, and PlGF isoforms (PlGF-1, PlGF-2, and PlGF-3; refs. 5, 6) bind specifically to Flt-1 (7, 8). Flt-1 is expressed as a full-length tyrosine kinase receptor or as a soluble form carrying only the extracellular domain. Although VEGF binds to Flt-1 with a 10-fold higher affinity than to VEGFR-2/Flk-1, Flt-1 tyrosine kinase activity is very weak and does not induce biological activities, such as proliferation or migration in endothelial cells (7, 9). Gene targeting studies have highlighted the function of Flt-1 in the formation of blood vessels. Flt-1 null mutation resulted in early embryonic death with severe defects in the vascular and hematopoietic system (10). On the other hand, it has been shown that mice lacking the tyrosine kinase domain (Flt-1 TK−/−) develop generally normal but display an impairment of macrophage function (11). Several studies suggest that Flt-1 and its soluble form might act as a decoy receptor by trapping VEGF-A, being therefore essential in regulating the amount of VEGF available to bind to VEGFR-2/flk-1 (12, 13).

Flt-1 is expressed not only by vascular endothelial cells but also by monocytes and macrophages (14–16). Moreover, other nonendothelial cells were reported to express Flt-1, including smooth muscle cells (17), trophoblasts (18), osteoblasts (16), and microglia (19).

The role of Flt-1 signaling in supporting pathologic angiogenesis has been shown in several pathologic conditions such as tumorigenesis (20), metastasis (21), and inflammatory diseases (22). Although these studies have clearly defined an important role of Flt-1 in pathologic angiogenesis, they could not differentiate the biological role of Flt-1 signals at level of endothelial cells and the functional importance of Flt-1 signaling in tissue-infiltrating macrophages. In brain tumors, such as glioblastomas, macrophage/microglia infiltration is found to be abundant within the tumor (23). A large amount of evidence suggests that macrophage/microglia are also equipped to perform tasks that will help the gliomas to become more invasive and to grow further, having an essential function in supporting tumor angiogenesis (24). In several tumor types, including glioblastomas, macrophage infiltration has been associated with poor prognosis. Flt-1 could be involved in macrophage-mediated tumor growth via at least two mechanisms: First, via Flt-1-kinase–dependent macrophage activation and

Note: Supplementary data for this article are available at Cancer Research Online (http://cancerres.aacrjournals.org/).

Requests for reprints: Marcia Machein, Department of Neurosurgery, Neurocenter, University of Freiburg, Breisacher Straβe 64, 79106 Freiburg, Germany. Phone: 49-761-2705147; Fax: 49-761-2705147; E-mail: Marcia.machein@uniklinik-freiburg.de.

doi:10.1158/0008-5472.CAN-07-6241

expression of several proangiogenic factors (25); second, Flt-1 might be able to mediate the migration of monocytes toward VEGF-A and PlGF. In this study, we analyzed the importance of Flt-1 signaling in tumor-infiltrating macrophages/microglia in a murine glioma model and its relevance for tumor growth and neoangiogenesis.

Materials and Methods

Cell Lines, Plasmid Construction, and Cell Transfection

Murine glioma Gl261 cells were kindly provided by Dr. Gaetano Finnocchiaro (Instituto Nazionale Neurologico "Carlo Besta," Milan, Italy). GP+E86 virus–producing cells were provided by Dr. Georg Breier (Department of Pathology, University of Dresden). Cells were cultured in DMEM supplemented with 10% FCS.

The generation of Gl261-VEGF has been previously described (26). For generation of Gl261-PlGF, a full-length human PlGF-2 cDNA was inserted into a pLEN retroviral vector and used to stably transfect GP+E86 virus–producing cells. The transfected cells were selected with 1 mg/mL neomycin analogue G418. High-titer retroviruses were used to infect Gl261 murine glioma cells as previously described (26). G418-resistant clones were screened for the expression of PlGF based on Northern and Western blot analyses. Retrovirus supernatant expressing an empty pLEN vector was used to generate Gl261-empty vector. G418-resistant clones were examined by reverse transcription-PCR for the expression of the neomycin gene. No major differences were observed in the *in vitro* cell proliferation among Gl261, Gl261-empty-vector, Gl261-VEGF, and Gl261-PlGF.

RNA Isolation

RNA extraction from tumor samples was carried out in two steps: Frozen tumor samples were homogenized in 1 mL PeqGold RNA Pure reagent (PeqLab Biotechnology). Next, 200 μL of chloroform were added to the homogenized sample and centrifuged (12,000 × *g*, 15 min, and 4°C). The resulting aqueous supernatant was mixed with 1 volume isopropanol and centrifuged (12,000 × *g*, 10 min, 4°C). After this step, the pellet was resuspended in 350 μL of RTL buffer and further purified using the Qiagen RNA mini kit (Rneasy total kit, Qiagen) according to the manufacturer's instructions. The concentration of each sample was obtained from A_{260} measurements. RNA integrity was tested by gel electrophoresis.

Reverse Transcription and Real-time PCR

One microgram (1 μg) of total RNA from tumors was reverse transcribed using RT2 First Strand Kit (Superarray Bioscience Corporation) according to the manufacturer's procedures. This kit contains a procedure to eliminate contaminating genomic DNA from RNA samples before reverse transcription.

Mouse SDF-1 (CXCL12) Taqman assay (Mm0044552-m1, Taqman Gene Expression Assay, Applied Biosystems), which recognized the three isoforms of mouse SDF-1 (reference sequences NM001012477.1, NM013655.3, NM021704.2, amplicon length 122), was used in the present study. Real-time PCR was performed in triplicate in optical multiwell plate 384 using Light Cycler 480 Probes Master (Roche Applied Science). For each 20 μL Taqman reaction, 2 μL cDNA samples (diluted 1:10, 1:100, which corresponding approximately to the cDNA from 10 and 1 ng RNA, respectively) were mixed with the reaction solution (18 μL) consisting of 1 μL primer-probe mix, 10 μL 2× Light Cycler 480 Probe Master, and 7 μL of water, PCR grade. For endogenous control, parallel assays for each sample were carried out using primers and probes for β-actin (Mm00607939_s1) and for mouse phosphoglycerokinase (PGK-1; Mm00435617_m1; Applied Biosystems). Negative controls were performed with water and RNA without reverse transcription. The reaction was carried out in a LightCycler 480 System (Roche Applied Science) using the following parameters: preincubation 95°C for 5 min, amplification 45 cycles (95°C for 10 s, 60°C 30 s). Standard curves were prepared using four dilutions of representative tumor probe known to express high amounts of SDF-1 and prepared for SDF-1, β-actin, and PGK-1. Relative mRNA levels (arbitrary units) of SDF-1 from two different probes per group (mock-transfected, VEGF-overexpressing tumors and PlGF-overexpressing tumors) were normalized against β-actin and PGK-1.

Northern Blot Analysis

Five to 10 μg of RNA were electrophoresed in a 1.5% agarose gel containing 15% formaldehyde and subsequently transferred to a Duralon membrane (Stratagene) in 10 × SSC. Filters were cross-linked with UV light (0.4 J/cm^2) and hybridized at 68°C in hybridization solution (QuickHyb, Stratagene) with the following random-primed ^{32}P-labeled cDNA probes: a cDNA 550-bp fragment encoding for the human PlGF-2, a 350-bp cDNA fragment encoding for $VEGF_{164}$, and a 416-bp cDNA fragment encoding for murine SDF-1α.

Western Blot Analysis

Cells were cultured with 1% FCS for 72 h. Conditioned media were removed and filtered through a 0.45-μm filter (Millipore Corp.). The conditioned media were concentrated ~10-fold using Centricons with a 10-kDa cutoff (Amicon). Aliquots were separated on a 12% polyacrylamide gel and transferred to a polyvinylidene difluoride membrane. The membrane was incubated with a polyclonal rabbit anti–PlGF-2 antibody (ReliaTech GmbH) directed against the NH_2 terminus of hPlGF-2 protein (1:50) followed by incubation with a goat anti-rabbit antibody conjugated to alkaline phosphatase (1:10.000; Tropix Bedford). Visualization was performed using a chemiluminescence technique (CPD-Star, Tropix) according to the manufacturer's instructions and documented on a Kodak X-Omat AR film (Kodak, Ltd.).

Animals and Tumor Implantation

All experiments using animal models were carried out according to the approval of the local animal care committee. Mice Flt-1 TK−/− lacking the tyrosine kinase domain (11) were backcrossed with heterozygous green fluorescent protein (GFP) transgenic mice (ACTbEGFPOsb/J). Genotyping was performed as previously described (11).

Homozygote offsprings with a target inactivation of the tyrosine kinase domain of Flt-1 expressing ubiquitously GFP (Flt-1 TK−/− GFP) were used as bone marrow donors.

C57BL6 (6–8 wk old) obtained from the animal colony of the University of Freiburg were used as bone marrow recipients. Myeloablative conditioning was performed with a single lethal dose of 9 Gy total body irradiation from a cobalt source. Bone marrow cells were harvested by flushing femurs and tibias 6 to 8 wk Flt-1 TK−/−GFP. Unfractioned bone marrow cells (5×10^6) were inoculated i.v.

Seven to eight weeks post bone marrow transplantation, mice were anesthetized and syngeneic murine glioma Gl261 cells (0.8×10^5) were slowly inoculated intracerebrally into the right caudatus as previously described (26). Twelve days (PlGF- and VEGF-overexpressing tumors) or 20 days (wild-type tumors) after tumor implantation, mice were euthanized through cardiac perfusion. These different time points were chosen because of the development of symptoms related to the growing intracranial tumor in parental and VEGF- and PlGF-transfected tumors.

Brains were removed and either postfixed in 2% paraformaldehyde or snap frozen in liquid nitrogen–cooled *N*-methylbutane. To grow s.c. tumors, mice were given an injection at the side of 2×10^6 viable Gl261 cells suspended in 0.2 mL of PBS/Matrigel (2:1).

Peripheral Blood Analysis

Blood was collected at the time of autopsy through cardiac puncture and white cell count was determined using an automated hematology analyzer (Cell-Dyn 3500). Donor-derived hematopoietic contribution (percentage of GFP+ cells in peripheral blood) was measured by flow cytometric analysis at the time of tumor implantation and at the time of autopsy.

Magnetic Resonance Imaging and Evaluation of Tumor Volume

On day 12 and 20 after tumor implantation, the animals were anesthetized with 2% isofluorane (Abbott GmbH & Co. KG) in a 20/80 oxygen/air gas stream. A Bruker Pharma Scan 7.0 T MR imager (300.51MHz for ^{1}H, 300 mT/m gradient system) was used to acquire images in T1-weighted [TR = 451.4 ms, TE = 5.5 ms, 1 acquisition (NEX 1 averages), TA = 1 min 55 s, field of view = 2.7 × 2.7 cm, matrix = 256 × 256, slice thickness = 1.00 mm, voxel size = 10.5 × 10.5 × 1 mm^3] and T2-weighted

Table 1. Effect of Flt-1 signals in macrophages on Gl261 intracranial gliomas

Analysis parameters	Intracranial implanted tumor in bone marrow chimeras					
	Gl261-WT		GL261-VEGF		GL261-PlGF	
	Flt-1 TK+/+	Flt-1 TK−/−	Flt-1 TK+/+	Flt-1 TK−/−	Flt-1 TK+/+	Flt-1 TK−/−
Tumor volume (mm^3) [MRI]						
Day 12	15.9 ± 9.9* (n = 5)	2.76 ± 1.0 (n = 5)	42.1 ± 27 (n = 5)	25.1 ± 18.4 (n = 6)	26.6 ± 12.3* (n = 6)	10 ± 7.9 (n = 8)
Day 20	67.7 ± 37.07* (n = 5)	21.25 ± 13 (n = 5)				
Tumor volume (mm^3) [histology]						
Day 12			98.1 ± 40.7 (n = 5)	92 ± 77.4 (n = 5)	20.9 ± 17.1 (n = 5)	8.1 ± 7.9 (n = 6)
Day 20	82.6 ± 51.7 † (n = 10)	15.4 ± 17.4 (n = 10)				
Vessel density (%)	9.21 ± 1.92* (n = 4)	5.28 ± 1.18 (n = 4)	11.1 ± 1.41 (n = 6)	10.62 ± 1.6 (n = 4)	9.31 ± 2.29 (n = 3)	7.69 ± 1.1 (n = 5)
GFP infiltration (%)	1.27 ± 0.86 (n = 4)	0.69 ± 0.25 (n = 4)	3.9 ± 0.3 † (n = 4)	1.11 ± 0.48 (n = 4)	3.43 ± 0.73* (n = 5)	2.33 ± 0.43 (n = 6)
Vessel permeability (k_{ep} [1 min^{-1}])	3.52 ± 3.4 (n = 3)	3.35 ± 1.6 (n = 4)	6.7 ± 4.9 (n = 4)	6.3 ± 4.8 (n = 4)	2.71 ± 2.1 (n = 2)	2.7 ± 2.36 (n = 2)
WBC count (Ts/μL)	5.04 ± 1.28 (n = 5)	3.38 ± 0.46 (n = 5)	4.40 ± 2.1 (n = 5)	6.81 ± 1.36 (n = 4)	5.4 ± 3.2 (n = 4)	3.93 ± 0.99 (n = 4)

NOTE: Data represent mean ± SD. Tumor volume was assessed by means of MRI and histologic analysis. Vessel density was determined in at least eight CD31-stained sections per animal. GFP infiltration was evaluated in at least eight tumor-containing coronal sections per animal. Vessel permeability was determined *in vivo* by DCE-MRI.

*$P < 0.05$.

† $P < 0.01$.

[TR = 3081.0 ms, TE = 72.0 ms, 1 acquisition (NEX 1 averages), TA = 6 min 34 s, field of view = 2.5 × 2.5 cm, matrix = 512 × 128, slice thickness = 1.5 mm, voxel size = 4.9 × 19.5 × 1.5 mm^3] images using spin echo sequences. Coronal serial T2-weighted scans were obtained before contrast medium injection. The mice received a dose of 80 μL i.p. of gadolinium DPTA (Magnevist, Bayer-Schering Pharma, Deutschland GmbH) and T1-weighted scans were taken for 10 min.

Tumor size was calculated in T1-weighted image sets obtained 10 min after contrast injection. The slices that showed enhanced areas were analyzed by defining a region of interest around the section of enhancement and measuring the area. The volume was calculated by multiplying by the slice thickness. This procedure was repeated for all slices showing enhancement and the areas were summed to determine a total tumor volume.

Immunofluorescence, Histochemistry, and Morphometry

Paraformaldehyde-fixed (2%) 50-μm vibratome sections (Leica VT-1000S, Leica Microsystems AG) were stained with the following antibodies: rat anti-mouse VEGFR-1 (1:100, R&D Systems), rabbit anti-human von Willebrand factor (vWF; 1:100, Dako), and rat anti-mouse F4/80 (1:100, Serotec), as previously described (26). Cryosections were stained with mouse anti-mouse/human SDF-1α (1:60, R&D Systems), with a mouse anti-smooth muscle actin (SMA; 1:500, Sigma) and with a rat anti-mouse CD31 (1:100, Southern Biotech). To avoid unspecific binding with mouse anti–SDF-1α, MOM Kit (Vector Laboratories, Inc.) was used according to the manufacturer's instructions. Antibody against SMA was directly labeled with AlexaFluor647 using Monoclonal Antibody Labeling Kit followed the manufacturer's instructions (Invitrogen). Sections were incubated with appropriate secondary antibodies, mounted, and analyzed with krypton-argon laser scanning confocal imaging system (TCSNT, Leica Microsystems AG).

Tumor volume. Paraformaldehyde-fixed brains were cut in sections 50-μm apart. Every fifth slide was stained with hematoxylin to identify intracranial tumor. The glioma volume was estimated by measuring the tumor area in each section using the bright field of a Leica microscope equipped with a digital camera and was analyzed with the Image 1000 analysis software. Total volume was calculated based on the number of tumor-containing sections × 50 μm × the area estimated in each section.

Vessel density. To quantify the tumor vascularization, CD31-stained representative random fields within tumor tissues were visualized at ×20 magnification. Photomicrographs were analyzed with Cell P Imaging-Software (Olympus). The vessel density is defined as percentage of vessel area within tumor area.

Quantification of bone marrow–derived myeloid cell infiltration in tumor tissue. To quantify the number of tumor-infiltrating GFP+ cells, each fifth to tenth vibratome section was mounted and imaged using the confocal microscope. To analyze the GFP cell count, random micrographs were taken throughout the tumor at ×40 magnification. For analysis of the GFP area fraction, tumor tissue was visualized at ×5 magnification. The absolute number of GFP+ cells and the GFP+ area in the tumor tissue were quantified using Image J software.

Monocyte Chemotaxis

Peripheral blood was collected through cardiac puncture of right ventricle in narcotized mice. Heparin was used as an anticoagulant. Blood was diluted 1:2 and subjected to density-gradient centrifugation using Histopaque-1077 (Sigma). Monocytes were further enriched using anti-mouse CD11b magnetic microbeads (Miltenyi Biotechnologies). Chemotaxis was studied using modified Boyden chamber (Whatman) adapting the protocol described for chemotaxis of human monocytes (27). In brief, isolated monocytes were resuspended in RPMI 1640. Chemo-attractants were loaded in the lower chamber, and cell suspension was

loaded in the upper chamber. Cells migrated across membrane with 5-μm pore size. Chemotaxis was allowed to proceed for 3 h at 37°C. Membranes were fixed in 100% ethanol and stained with Giemsa's azur eosin methylene blue solution (Merck). Cells adherent to the upper surface of the membrane were carefully scraped. The membrane was mounted onto microscopic slide with superimposed cover slide. Cells adherent to the lower surface of the membrane were referred as migrated. Migrated cells were counted in the whole well, at magnification of ×40. In each experiment, experimental condition was done in duplicate.

Dynamic Contrast-Enhanced Magnetic Resonance Imaging

Functionality and maturation aspects of the tumor neovasculature were investigated by dynamic contrast-enhanced magnetic resonance imaging (DCE-MRI) using a custom-developed transmit/receive small animal coil in a conventional whole-body 1.5 T MRI scanner (Symphony, Siemens). Brain tumors were located on T2-weighted turbo spin echo images (TE = 59 ms, TR = 1510, matrix = 96 × 128, voxel size = 0,4 × 0,4 × 1 mm^3). The change in signal intensity on identical T1-weighted MR images after injection of contrast media (Gadomer, Bayer Schering Pharma, 0.1 mmol/kg body weight) was recorded at the MR slice showing the largest tumor diameter. Using a FLASH (Fast Low Angle Shot) three-dimensional sequence (TR = 8 ms, TE = 2.6 ms, flip angle α = 25°, matrix = 128 × 64, voxel size = 0.4 × 0.4 × 1.0 mm^3), 70 dynamic scans with 30 slices per slab were performed within 13 min. As contrast agent 100 μL Gadomer (Schering, 0.1 mmol/kg body weight) was administered in the tail vein of narcotized (Isofluoran 1,5%, oxygen 98,5%) mice. Post contrast high-resolution T1-weighted imaging was performed using a spin echo sequence (TE = 2.6 ms, TR = 8.0 ms, matrix = 240 × 512, voxel size = 0.4 × 0.4 × 1.0 mm^3). Postprocessing of DCE-MRI data was performed using the pharmacokinetic two-compartment model described by Brix and

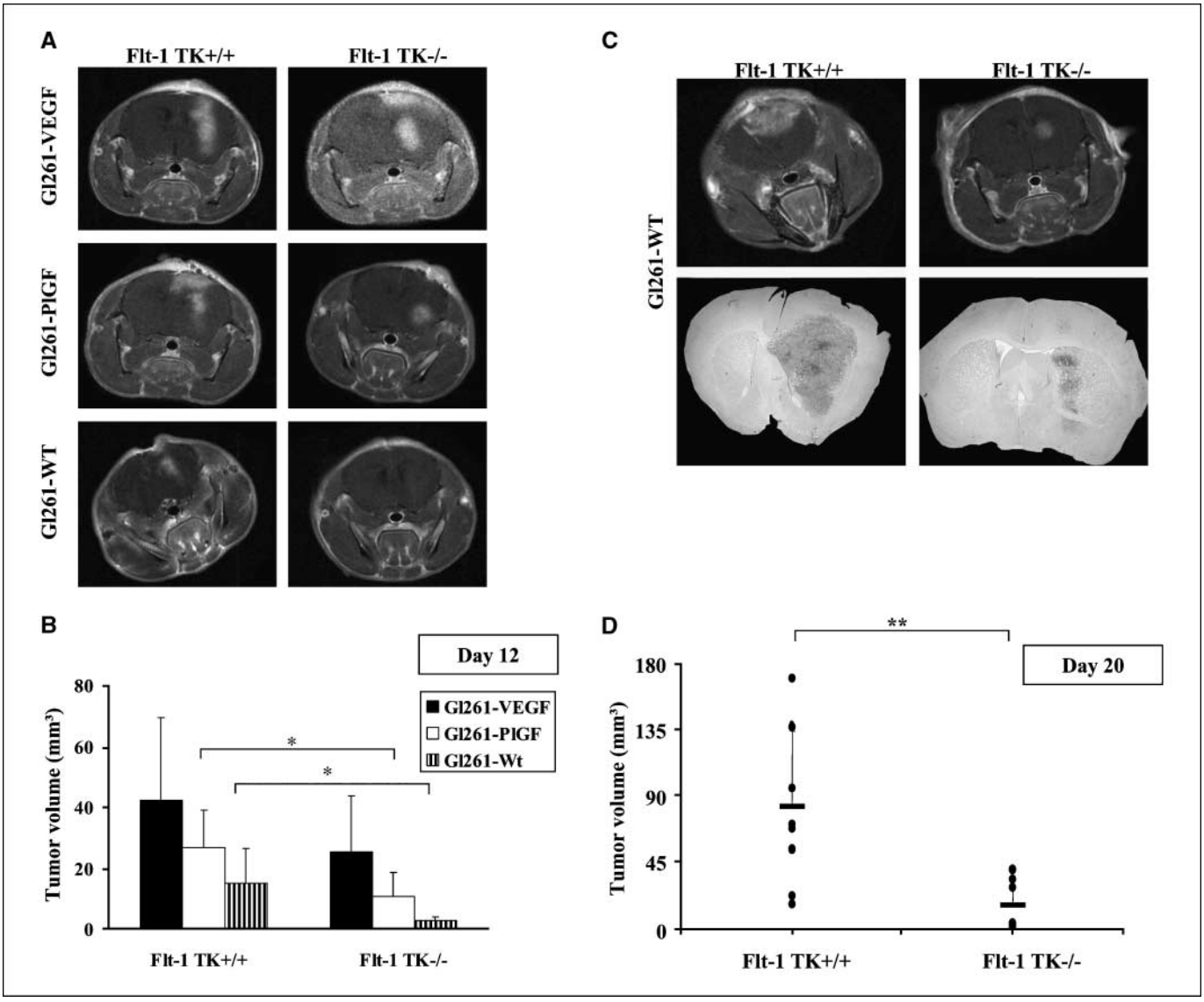

Figure 1. Deficiency of tyrosine kinase of Flt-1 in macrophages suppressed tumor growth *in vivo*. *A,* contrast-enhanced T1-weighted magnetic resonance images at day 12 after intracranial implantation of parental (*Gl261-WT*), VEGF-overexpressing (*Gl261-VEGF*), or PlGF-overexpressing (*Gl261-PlGF*) murine glioma cells in Flt-1 TK+/+ and Flt-1 TK−/− bone marrow chimeras. *B,* quantitative analysis of tumor volume obtained from MRI analysis: Wild-type tumors and PlGF-induced tumors in Flt-1 TK+/+ mice grew significantly faster than those in Flt-1 TK−/− animals (*, $P < 0.05$). *C,* contrast-enhanced T1-weighted MR images and histologic analysis of animals implanted with wild-type cells on day 20 postimplantation. The images obtained from histologic sections confirm the MR results and clearly show the significantly decreased tumor size in Flt-1 TK−/− compared with Flt-1 TK+/+ mice. *D,* growth inhibition of intracranial gliomas growing in Flt-1 TK−/− chimeras. Animals were sacrificed 20 d after intracranial injection of wild-type Gl261 glioma cells and tumor volume was determined histologically. Data were obtained from 10 mice per group. Tumor volume was significantly decreased in Flt-1 TK−/− bone marrow chimeras (**, $P < 0.01$).

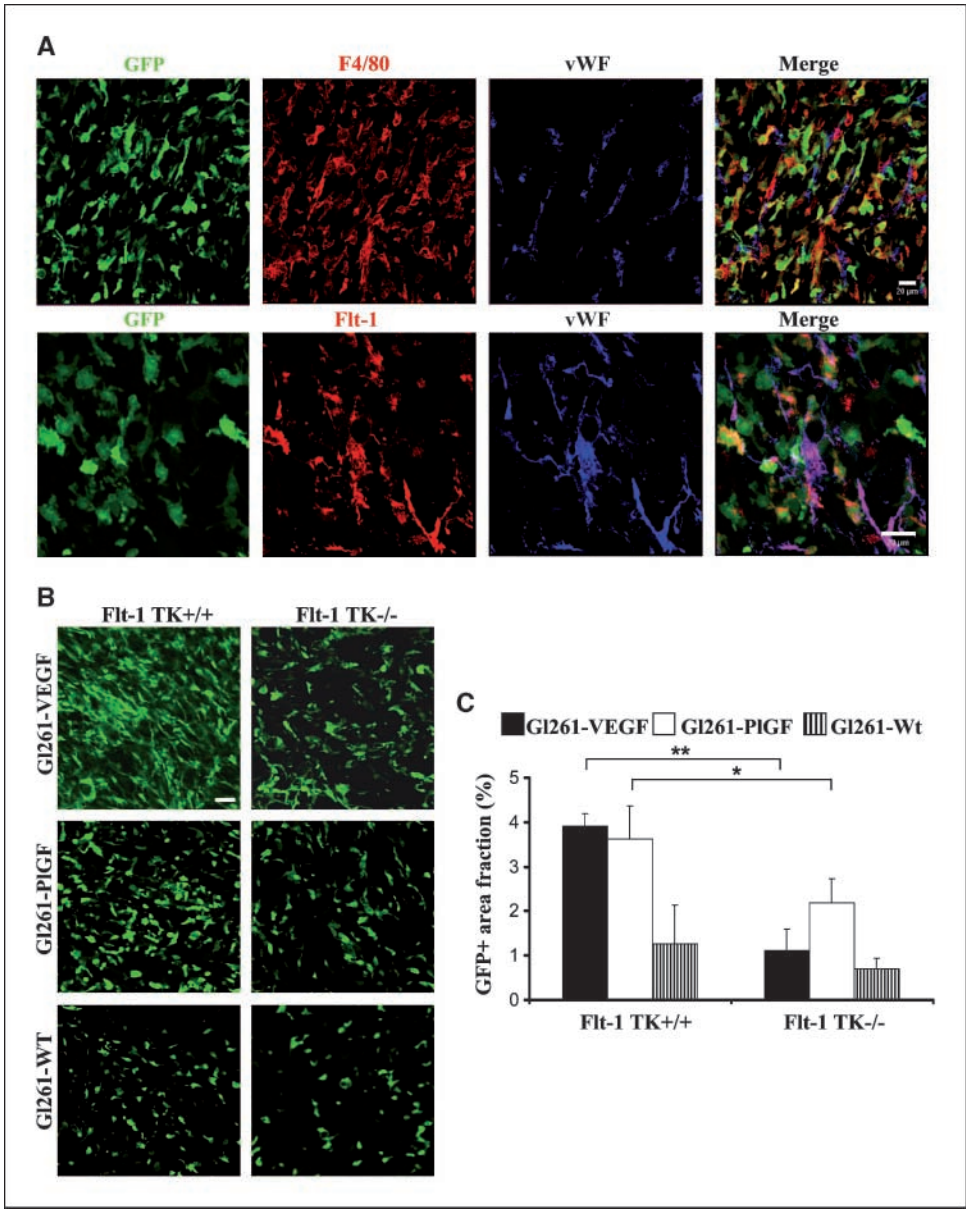

Figure 2. Involvement of Flt-1 receptor in macrophage migration. *A,* representative confocal micrographs of intracerebral tumors in Flt-1 TK−/− bone marrow chimeras. GFP-positive cells (*green*) coexpressed macrophage/microglia marker F4/80 and Flt-1 receptor (*red*). Tumor blood vessels were stained with vWF (*blue*). *Bar,* 20 μm. *B,* representative confocal pictures of infiltrating GFP+ bone marrow–derived cells into tumor sites of Flt-1 TK+/+ and Flt-1 TK−/− bone marrow chimeric mice. *Bar,* 20 μm. *C,* quantification of GFP+ area fraction was performed using computer-assisted morphometric analysis and calculated based on the examination of an average of 5 to 10 sections per animal (depending on tumor size). *Columns,* mean; *bars,* SD. Significant decrease of GFP+ infiltrating cells in Flt-1 TK−/− was observed in VEGF-overexpressing (**, $P < 0.01$) and PlGF-overexpressing tumors (*, $P < 0.05$). No major differences in GFP infiltration in parental tumors were detected between the Flt-1 TK−/− and Flt-1 TK+/+ bone marrow chimeras.

colleagues (28). To achieve color-coded parameter maps, the amplitude A (proportional to the contrast agent dose D and the fraction of blood volume to voxel volume) and the exchange rate constant k_{ep} (describing the exchange of contrast media between the intravascular and interstitial compartment) were calculated pixelwise and color-coded using the Dynalab (MEVIS, Bremen) software.

Statistical Analysis

All the statistical analyses were performed using SPSS 13.0 software. The statistical significance of the results was tested by Student's t test (unpaired two-tailored). A P value of <0.05 was considered statistically significant.

Results

Suppression of glioma growth in Flt-1 TK−/− bone marrow chimeras. To investigate whether Flt-1 signaling in bone marrow–derived myeloid cells is important for glioma growth and angiogenesis, we transplanted unfractioned bone marrow cells from Flt-1 TK−/− or Flt-1 TK+/+ expressing GFP into lethally irradiated syngeneic recipients. After bone marrow transplantation, Flt-1 TK+/+ and Flt-1 TK−/− bone marrow chimeras displayed comparable amounts of WBC (Table 1). The efficacy of donor cell engraftment as assessed by the percentage of GFP+ cells in peripheral blood was in average 80% (data not shown).

The growth rate of tumors was monitored using contrast-enhanced MRI at days 12 and 20 after implantation. Twelve days after tumor inoculation, tumors growing in Flt-1 TK+/+ bone marrow chimeras had small visible tumors, whereas tumors growing in Flt-1 TK−/− were barely detectable (Fig. 1*A* and *B*; Table 1). At day 20 postimplantation, tumor growth in Flt-1 TK+/+ was significantly larger than in Flt-1 TK−/− (Fig. 1*C* and *D*; Table 1). The experiment was repeated and tumor volumes were determined histologically in further experiments. Consistently, Flt-1 TK+/+ mice formed significantly larger tumors (~5-fold increase) than Flt-1 TK−/− animals (n = 10/group; $P < 0.05$; Table 1; Fig. 1*C* and *D*).

VEGF overexpression restores tumor growth in Flt-1 TK−/− bone marrow chimeras. To examine the effect of VEGF on tumor

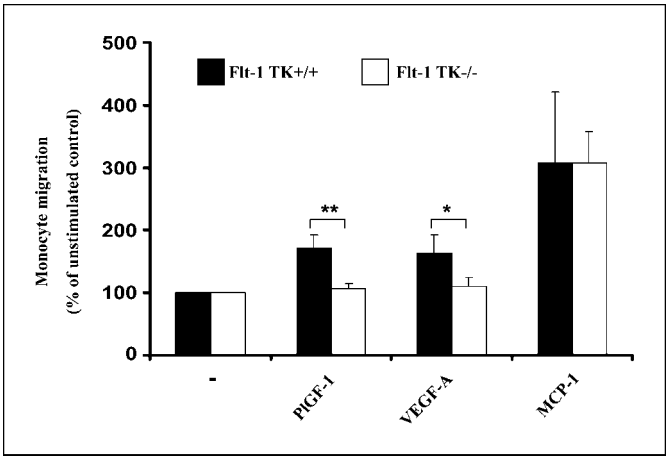

Figure 3. Assessment of mouse monocyte chemotaxis in Flt-1 TK−/− mice. Monocytes were isolated from heparinized mouse venous blood, taken from the right ventricle of the beating heart. Chemotaxis was assessed in the modified Boyden chamber at 37°C for 3 h. Chemoattractants (PlGF-1, VEGF-A, and MCP-1, 1 ng/mL) were loaded in the lower compartments, whereas cell suspensions were loaded in the upper compartments. Cells migrated across the membrane with 5-μm pore size. Migrated cells were counted using a light microscope (magnification, ×40). Data shown are derived from three independent experiments each performed in duplicate. Chemokinesis is referred as 100%. *Columns,* mean; *bars,* SD (*, $P < 0.05$; **, $P < 0.01$).

growth in Flt-1 TK+/+ and Flt-1 TK−/− bone marrow chimeras, mice were injected with glioma cells overexpressing $VEGF_{164}$ (Gl261-VEGF). Tumor growth was analyzed by MRI on day 12 postimplantation. As shown in Fig. 1 and Table 1, tumor volumes in the chimeric genotypes are similar (either in tumors studied by means of MRI or in tumors studied by histologic analysis), suggesting that VEGF overexpression by tumor cells alone can restore tumor growth in Flt-1 TK−/− chimeras (Fig. 1*A* and *B*; Table 1).

Effect of PlGF overexpression on tumor growth. To investigate the function of Flt-1 on myeloid cells in the presence of its ligand, PlGF, we generated stable transfectants of Gl261 cells overexpressing human PlGF-2 isoform. The mouse *PlGF* gene is homologous to hPlGF-2. Transfected clones displayed high levels of PlGF expression at mRNA and protein levels, whereas in parental or mock-transfected cells, no expression was detectable (Supplementary Fig. S1). Compensatory changes in endogenous VEGF levels were not seen by Northern blot analysis (Supplementary Fig. S1). Mice injected with PlGF-transfected cells into the brain were scanned on day 12 after injection. At this time, mice implanted with PlGF-overexpressing cells developed significantly larger tumors (median volume = 26.6 $mm^3 \pm 12.3$; $n = 6$) in Flt-1 TK+/+ chimeras compared with the reduced growth of intracranial tumors in Flt-1 TK−/− chimera (median volume = 10.0 $mm^3 \pm 7.9$; $n = 8$; Fig. 1*A* and *B*; Table 1). Compared with the wild-type tumors, PlGF-overexpressing cells developed larger tumor volumes at day 12 postimplantation although this difference did not reach statistical significance. These results indicate that PlGF overexpression might induce glioma growth and VEGFR-1 signaling in monocytes is important to stimulate this growth.

Homing of myeloid cells in response to VEGF and PlGF is impaired in Flt-1 TK−/− chimeras *in vivo*. At the time of autopsy (day 12 in PlGF-VEGF–overexpressing tumors and day 20 in parental tumors), the vast of majority of GFP+ cells that infiltrate the tumor tissue differentiated into macrophage/microglia characterized by immunoreaction for the macrophage marker F4/80 and expressed Flt-1 (Fig. 2*A*). To evaluate whether Flt-1 signaling in bone marrow–derived myeloid cells affects their recruitment into murine glioma, we used computer-assisted morphometry to analyze the percentage of GFP+ area within tumor tissue at low magnification. Inflammatory infiltration was also confirmed by counting the absolute number of GFP+ cells in random areas throughout the tumor (Fig. 2*B*). We found that in wild-type tumors,

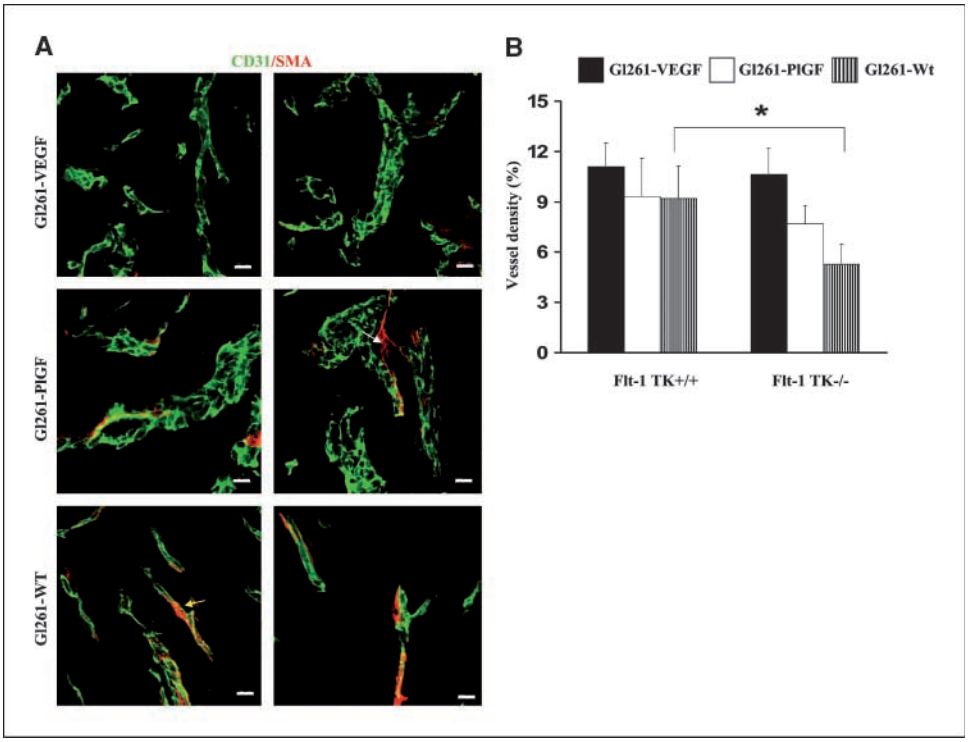

Figure 4. Comparison of the vascularity of Gl261-WT, Gl261-VEGF, and Gl261-PlGF tumors. *A,* double immunoflourescence staining of tumor vessels was performed using an antibody against SMA and an antibody against CD31. SMA coverage is visualized in red and tumor endothelial cells are visualized in green. VEGF-overexpressing cells generated vessels of irregular caliber and devoid of SMA-cell coverage. Overexpression of PlGF-originated vessels of large caliber with SMA+ cells partially loosely apposed to the endothelial cell layer (*white arrow*). In contrast, wild-type tumors disclosed vessels with SMA+ cells closely associated to the endothelium (*yellow arrows*). *Bar,* 20 μm. *B,* morphometric analysis of tumor vascularization was evaluated using CD31-stained sections within tumor tissue visualized at ×20 magnification. An average of 5 to 10 random fields per animal was analyzed. Photomicrographs were analyzed with the Cell P imaging software. Vessel density is defined as percentage of vessel area with tumor area. *Columns,* mean; *bars,* SD (*, $P < 0.05$). Tumor vascularization is significantly reduced in Flt-1 TK−/− chimeras implanted with parental Gl261 cells.

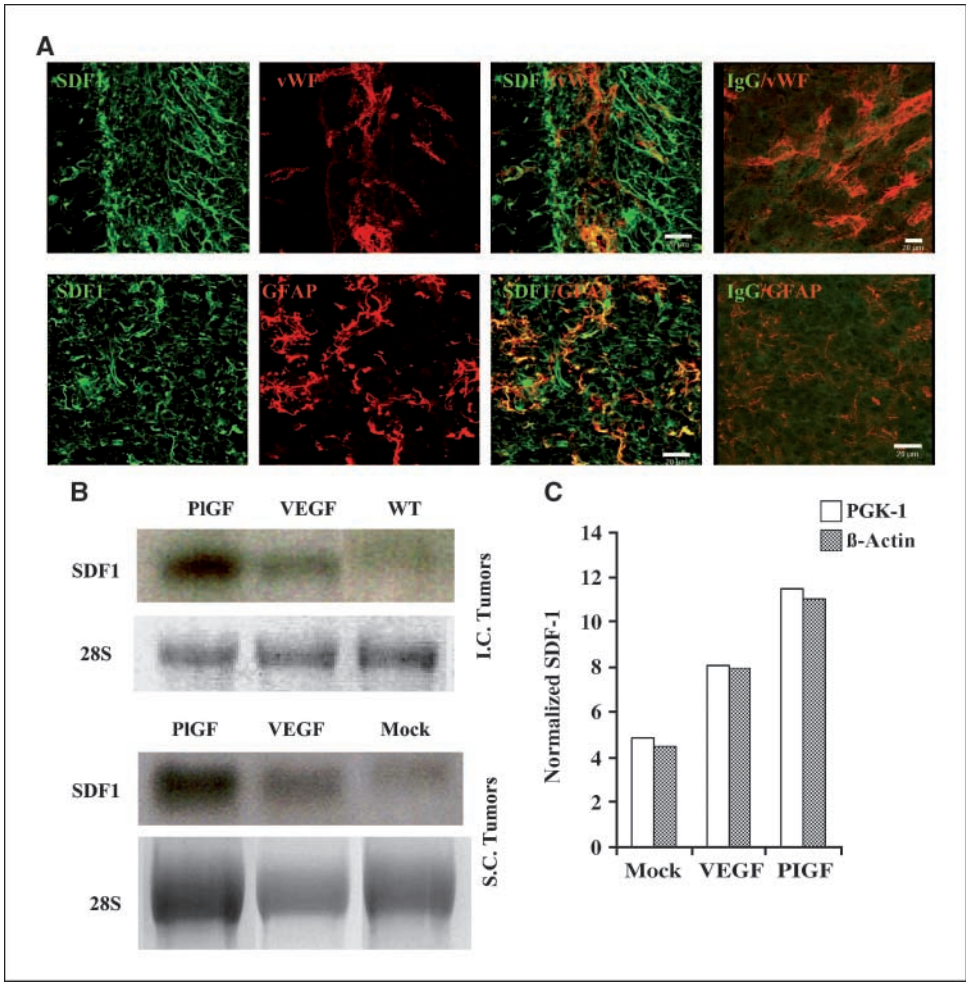

Figure 5. Increase of SDF-1 expression by PlGF and VEGF overexpression. *A,* double immunostaining for SDF-1/CXCL12 (*green*) and vWF (*red*) and for SDF-1/CXCL-1 (*green*) and GFAP (*red*) in intracranial gliomas. Mouse nonspecific IgG (*green*) was used as negative control. SDF-1/CXCL12 is expressed by tumor cells, by reactive astrocytes, and, to lesser extent, by endothelial cells. *Bar,* 20 μm. *B,* Northern blot analysis of intracranial (*I.C.*) and subcutaneous (*S.C.*) tumors (*cropped blots*) implanted with Gl261-PlGF, Gl261-VEGF, Gl261-WT, and Gl261-empty vector (full-length gels are presented in Supplementary Fig. S2). *C,* real-time PCR analysis for SDF-1 in Gl261 tumors. Relative quantification showed elevated levels of SDF-1 mRNA in PlGF-overexpressing (normalized against PGK-1: 11.46 ± 3.4 and against β-actin: 10.98 ± 1.52) and VEGF-overexpressing (normalized against PGK-1: 8.06 ± 2.49 and against β-actin: 7.9 ± 2.6) tumors compared with mock-transfected tumors (normalized against PGK-1: 4.85 ± 2.0 and against β-actin: 4.45 ± 1.4).

the inflammatory infiltration represented by GFP+ cells did not significantly differ between the two genotypes. Inducing VEGF and PlGF expression in tumor tissues led to a massive infiltration of GFP+ cells (3.1-fold and 2.7-fold increase compared with the infiltration in tumors generated by implantation of wild-type glioma cells), confirming previous reports that VEGF and PlGF act as a potent chemoattractant factors for monocytes/macrophages. In VEGF- and PlGF-overexpressing tumors, we determined a significant decrease in the number of infiltrating GFP+ macrophages in Flt-1 TK−/− bone marrow chimeras (Table 1; Fig. 2*C*).

In vitro, as shown in Fig. 3*A*, VEGF- and PlGF-induced monocyte migration was strongly abrogated in monocytes isolated from Flt-1 TK−/− mice, although these monocytes responded to monocyte chemoattractant protein-1 (MCP-1) in the same assay. These observations suggest that Flt-1 is required for monocyte/macrophage migration *in vitro* and *in vivo* in the presence of high amounts of its ligands.

Regardless of whether the tumors overexpressed VEGF or PlGF, we did not observe GFP+ cells that participated in blood vessel formation by differentiation into vascular cells, confirming our previous studies that glioma vascularization is essentially derived from the proliferation of endothelial cells (data not shown).

Deficiency of Flt-1 signals in bone marrow–derived myeloid cells decreases vessel density in wild-type tumors, but not in PlGF- or VEGF-overexpressing tumors. Tumor vascularization was then analyzed at the time of autopsy (wild-type tumors on day 20, VEGF- and PlGF-overexpressing tumors on day 12 postimplantation, when mice developed symptomatic tumors) by immunofluorescence using an antibody against the endothelial cell–specific marker CD31 and against the SMA, which detects mural cells surrounding endothelial cells (Fig. 4*A*). Tumor angiogenesis induced by PlGF-transfected glioma cells seemed to be less dependent on sprouting (angiogenesis) but occurred via an increase in the diameter of blood vessels. However, no significant increase in vessel density as compared with wild-type tumors was observed. This pattern of enlarged vessel was more accentuated in s.c. than in intracerebrally grown tumors (data not shown). Large vessels in PlGF-overexpressing tumors have a clear layer of SMA-positive cells, which seemed to be partly loosely apposed to the endothelial cell layer (Fig. 4*A*). In wild-type tumors retrieved from Flt-1 TK−/− bone marrow chimeras, the vessel density was significantly reduced by 43% (n = 4/group; P = 0.04). VEGF-overexpressing tumors showed a similar vessel density in both genotypes. PlGF-overexpressing tumors disclosed a reduction of tumor neovasculature by 15% in Flt-1 TK−/− bone marrow chimeras; however, this difference did not reach significance (Table 1; Fig. 4*B*). These results suggest that tumor vascularization in Flt-1 TK−/− bone marrow chimeras is restored by VEGF-A overexpression and is, at least in part, compensated by PlGF overexpression.

Induction of vascular hyperpermeability in VEGF- but not in PlGF-overexpressing tumors. Because increased edema formation has been linked to the amount of inflammation and the levels of PlGF and VEGF in tumors, we assessed the vascular permeability using DCE-MRI. VEGF-overexpressing tumors showed an increased vascular permeability (k_{ep} = 6.7 ± 4.9 min^{-1} in wild-type chimeras; 6.3 ± 4.8 min^{-1} in Flt-1 TK−/−). Permeability measurements in PlGF-overexpressing tumors by DCE-MRI showed a similar vascular permeability compared with the parental Gl261 tumors (Table 1). In wild-type, VEGF-overexpressing, and PlGF-overexpressing tumors, there are no major differences in levels of vascular permeability in Flt-1 TK−/− and Flt-1 TK+/+ bone marrow chimeras (Table 1), suggesting that Flt-1 signals in inflammatory cells did not influence edema formation in gliomas.

Increase of SDF-1 expression by PlGF and VEGF overexpression. SDF-1/CXCl12 (stromal cell–derived factor-1) is a chemokine involved in the regulation of hematopoietic cells. SDF-1 has been reported to be up-regulated by VEGF in perivascular cells, and SDF-1 induction is essential to retain hematopoietic cells in close proximity to angiogenic vessels (29). Immunohistochemical analysis showed SDF-1 protein being expressed not only by tumor cells but also by reactive astrocytes and the astrocyte foot processes predominantly around blood vessels. This was shown by the colocalization of SDF-1 with the astrocyte marker glial fibrillary acidic protein (GFAP). SDF-1 was also expressed to a lesser extent in the endothelium (Fig. 5*A*). SDF-1 mRNA levels were analyzed by Northern blot analysis and by using relative real-time PCR with β-actin and PGK-1 as an endogenous control in intracranial and s.c. tumors. Elevated levels of SDF-1 mRNA were found in PlGF-overexpressing and in VEGF-overexpressing tumors (2.4-fold and 1.7-fold increase, respectively) compared with wild-type and empty vector–transfected tumors (Fig. 5*B* and *C*).

Discussion

In this study, we show that loss of Flt-1 signaling in tumor-infiltrating macrophages has a profound suppressive effect on tumor growth and vascularization in an experimental glioma model. Gliomas implanted in wild-type bone marrow chimeras were larger and better vascularized than those grown in chimeras generated by transplantation of bone marrow cells derived from Flt-1 TK−/− mice. It was broadly accepted that the initial angiogenic switch is predominantly promoted by tumor cells, which became hypoxic through insufficient blood supply (30). However, it has been recognized that tumor cells cannot ensure the expression of angiogenic factors alone. A central role of inflammation in sustaining tumor angiogenesis has only recently become evident. Tumor-infiltrating leukocytes, including mast cells, neutrophils, and particularly macrophages, are important cellular sources of VEGF into critical points of tumor (31, 32). In normal tissue repair, recruited macrophages constitute the main source of VEGF and represent a fundamental step for initiating an effective angiogenic response (33). Moreover, macrophage depletion or suppression of inflammation with acetyl salicylic acid reduced ovarian tumor progression and ascites formation, which is closely related to reduction in VEGF protein levels in the ascites fluid (34). In several experimental tumors, evidence suggested that macrophage concentration correlates with capillary development and tumor growth (35). It has been shown that Flt-1 is expressed by other cell types, including monocytes/macrophages. Flt-1 signaling in macrophages has been implicated in promoting cell survival and migration (36). In addition, bone marrow–derived cells expressing Flt-1 have been shown to home to premetastatic sites and form cellular clusters, which promote metastasis growth (21). An antibody against Flt-1 suppressed the neovascularization in tumors and blocked the mobilization of myeloid cells *in vitro* and *in vivo* (37). A recent study has provided evidence for existence of an autocrine VEGF/Flt-1 loop in neuroblastoma cells, which promotes hypoxia-inducible factor (HIF-1) activation (38). Inhibition of VEGF/Flt-1 decreased HIF-1α phosphorylation. Such an autocrine loop linking VEGF/Flt-1 signaling with HIF-1 activation might be also functional in macrophages. Murakami and colleagues (22) have shown that secretion of VEGF upon stimulation with hVEGF is attenuated in macrophages derived from Flt-1 TK−/− mice. These data suggest that VEGF/Flt-1 in macrophages might serve to amplify expression of proangiogenic factors, including VEGF itself. Our observation that overexpression of VEGF but not of PlGF restores glioma growth in Flt-1 TK−/− chimera supported this interpretation.

Several groups have shown that Flt-1 is important for VEGF-dependent monocyte/macrophage migration (39). PlGF is also chemotactic for monocytes and can restore late phases of hematopoesis through chemotaxis of Flt-1–expressing bone marrow progenitor cells (40). We observed that implantation of glioma cells overexpressing VEGF-A or PlGF leads to a massive infiltration of the GFP cells into glioma tissue *in vivo*, which is significantly less extensive in Flt-1 TK−/− chimeras. Furthermore, we found that the inflammatory infiltration in wild-type gliomas represented by the number of GFP+ cells was similar in Flt-1 TK−/− and Flt-1 TK+/+ recruitment. A number of tumor-derived chemoattractants besides VEGF and PlGF ensures the recruitment of leukocytes into tumor tissue, including monocyte chemoattractant protein-1 (MCP-1); colony-stimulating factor-1 (CSF-1, also known as M-CSF); and the CC chemokines, CCL2, CCL3, CCL4, CCL5, and CCL8 (31, 41). Gl261 glioma cells express low basal levels of VEGF and PlGF. Thus, in parental Gl261 tumors with low basal levels of VEGF and PlGF, other chemokines might mediate the inflammatory infiltration and Flt-1 function might become redundant for macrophage. The infiltration of GFP+ cells in PlGF-overexpressing tumors in Flt-1 TK−/− chimeras showed some increase in comparison with wild-type and VEGF-overexpressing tumors growing in the Flt-1 TK−/− chimeras. This observation is in contrast to our *in vitro* data, which show that PlGF- and VEGF-induced chemotaxis is abrogated in monocytes without a functional Flt-1. A possible explanation for this discrepancy is that PlGF *in vivo* might induce other cells besides macrophages (for instance, endothelial cells) to produce chemokines responsible for inflammatory infiltration. We show in this study that PlGF overexpression *in vivo* increases the levels of SDF-1/CXCl12 even more potently than VEGF. It has been shown that SDF-1/CXCL12 up-regulation is an integral part of the angiogenic response triggered by VEGF to maintain hematopoietic cells closely associated with angiogenic vessels (29). Recent findings suggested that PlGF-induced mobilization of inflammatory cells to angiogenic sites might also be modulated by SDF-1/CXCl12 (42). Although several other stimuli, including hypoxia, are known to regulate SDF-1/CXCL12 expression, our results confirm previous findings that SDF-1/CXCL12 might be an important downstream target of VEGF and PlGF to recruit hematopoietic cells to tumor bed. Furthermore, the data presented here highlighted the importance of functional Flt-1 for VEGF- and PlGF-mediated bone marrow recruitment *in vivo*.

Here, we show that PlGF-overexpressing tumors are larger in Flt-1 TK+/+ than in Flt-1 TK−/− chimeras although these tumors exhibited no statistically significant difference in vessel density. Overexpression of PlGF-2 resulted in increase of tumor growth compared with control tumors. Regarding the contribution of PlGF to tumor growth, conflicting reports are found in the literature. In PlGF-deficient mice, tumor growth and angiogenesis are markedly reduced (43). Overexpression of PlGF through an inducible system increases tumor growth (36). On the other hand, it has been shown that PlGF might play a negative role on tumor growth and angiogenesis through formation of VEGF/PlGF heterodimers (44, 45). These discrepant results might be explained by the levels of VEGF and PlGF expressed by tumor cells: The antagonistic effect of PlGF in opposing VEGF requires coexpression of both factors by the same cell to form inactive heterodimers (44). Parental Gl261 tumors expressed constitutively low levels of VEGF, and Gl261-overexpressing PlGF did not increase the levels of endogenous VEGF; thus, the formation of inactive heterodimers in this tumor model is unlikely. Another mechanism to explain the growth of PlGF-overexpressing murine gliomas in Flt-1 TK+/+ chimeras is the intensive accumulation of macrophages observed in these tumors. This infiltration is significantly decreased Flt-1 TK−/− chimeras, which might explain the impaired tumor growth in these animals. Our study shows an overall protumor effect for PlGF, which seemed to be dependent on macrophage recruitment mediated by Flt-1.

VEGF and PlGF have been shown to increase vascular permeability (46, 47). A common feature of malignant gliomas is their ability to increase vascular permeability, which subsequently leads to vasogenic edema. Previous studies have shown that PlGF alone or in synergy with VEGF can substantially increase vascular permeability (48, 49). Using DCE-MRI, we showed in this study that VEGF overexpression as expected enhanced the vascular permeability whereas in PlGF-overexpressing tumors, values were comparable with parental tumors. Vascular leakage has been associated with vessel maturation. We found that PlGF-overexpressing tumors disclose vessels with larger diameters, which are covered by smooth muscle–positive cells, whereas in VEGF-overexpressing tumors staining for smooth muscle cells in tumor vessels were almost undetectable. The effect of PlGF on pericyte recruitment has previously been investigated in PlGF-deficient mice (43). These mice display less mature vessels than the control mice. Other studies report that vessels in PlGF-overexpressing tumors contain less SMA-positive cells compared with controls (20). Our findings are consistent with the hypothesis that PlGF induced the formation of large, mature, and less leaky vessels in intracranial gliomas, whereas VEGF formed immature, highly permeable tumor vascular network. This pattern is independent whether tumors grew in wild-type or in Flt-1 TK−/− bone marrow chimeras. The discrepancy found in the literature regarding PlGF expression and induction of tumor growth and vascular permeability highlighted the complexity of possible interactions of PlGF, which culminates with a protumorigenic or antitumorigenic effect.

The findings reported here highlight the relevance of Flt-1 expressed by macrophages in supporting glioma angiogenesis. We suggest that Flt-1 signaling in macrophages might be able to amplify the levels of available VEGF in the glioma tissue and may as such represent an important step particularly in the initial phases of tumor growth. Therefore, targeting Flt-1 receptor in bone marrow–derived infiltrating macrophages might be a promising approach to be used in the future antiangiogenic therapies in gliomas.

Disclosure of Potential Conflicts of Interest

No potential conflicts of interest were disclosed.

Acknowledgments

Received 11/14/2007; revised 4/16/2008; accepted 6/10/2008.

Grant support: Deutsche Krebshilfe grant 10-2224-Ma2 (M.R. Machein and K.H. Plate) and Deutsche Forschunggemeischaft (SFB-TR 23; Project C4 to M. Machein, C1 to K.H. Plate and Y. Reiss, and Z2 to F. Kiessling).

The costs of publication of this article were defrayed in part by the payment of page charges. This article must therefore be hereby marked *advertisement* in accordance with 18 U.S.C. Section 1734 solely to indicate this fact.

We thank Dr. Susanne Wizigmann-Voss for helping us with cloning procedures, Dr. Sabine Raab (Edinger Institut, Frankfurt, Germany) for genotyping analysis of Flt-1 tyrosine kinase mice, Prof. Dr. Gabriele Niedermann (Department for Clinical and Experimental Radiobiology, University Freiburg) for help with irradiation procedures, Dr. Mary Follo (Core facility, University Freiburg) for help with real-time PCR, Jasmin Droste and Christine Mayer for technical assistance, and Drs. Clemens Mueller (Kerckhoff Hospital, Bad Nauheim) and Astrid Wietelmann (Max-Planck-Institute for Heart and Lung Research, Bad Nauheim) for help with MRI measurements.

References

1. Carmeliet P. VEGF as a key mediator of angiogenesis in cancer. Oncology 2005;69 Suppl 3:4–10. Epub; 2005 Nov 21:4–10.
2. Shibuya M, Claesson-Welsh L. Signal transduction by VEGF receptors in regulation of angiogenesis and lymphangiogenesis. Exp Cell Res 2006;312:549–60.
3. Waltenberger J, Claesson-Welsh L, Siegbahn A, Shibuya M, Heldin CH. Different signal transduction properties of KDR and Flt1, two receptors for vascular endothelial growth factor. J Biol Chem 1994;269:26988–95.
4. Alitalo K, Carmeliet P. Molecular mechanisms of lymphangiogenesis in health and disease. Cancer Cell 2002;1:219–27.
5. Maglione D, Guerriero V, Viglietto G, et al. Two alternative mRNAs coding for the angiogenic factor, placenta growth factor (PlGF), are transcribed from a single gene of chromosome 14. Oncogene 1993;8:925–31.
6. Luttun A, Tjwa M, Carmeliet P. Placental growth factor (PlGF) and its receptor Flt-1 (VEGFR-1): novel therapeutic targets for angiogenic disorders. Ann N Y Acad Sci 2002;979:80–93.
7. Sawano A, Takahashi T, Yamaguchi S, Aonuma M, Shibuya M. Flt-1 but not KDR/Flk-1 tyrosine kinase is a receptor for placenta growth factor, which is related to vascular endothelial growth factor. Cell Growth Differ 1996;7:213–21.
8. Olofsson B, Korpelainen E, Pepper MS, et al. Vascular endothelial growth factor B (VEGF-B) binds to VEGF receptor-1 and regulates plasminogen activator activity in endothelial cells. Proc Natl Acad Sci U S A 1998;95:11709–14.
9. Shibuya M. Structure and dual function of vascular endothelial growth factor receptor-1 (Flt-1). Int J Biochem Cell Biol 2001;33:409–20.
10. Shalaby F, Rossant J, Yamaguchi TP, et al. Failure of blood-island formation and vasculogenesis in Flk-1-deficient mice. Nature 1995;376:62–6.
11. Hiratsuka S, Minowa O, Kuno J, Noda T, Shibuya M. Flt-1 lacking the tyrosine kinase domain is sufficient for normal development and angiogenesis in mice. Proc Natl Acad Sci U S A 1998;95:9349–54.
12. Yamaguchi S, Iwata K, Shibuya M. Soluble Flt-1 (soluble VEGFR-1), a potent natural antiangiogenic molecule in mammals, is phylogenetically conserved in avians. Biochem Biophys Res Commun 2002;291:554–9.
13. Chen H, Ikeda U, Shimpo M, et al. Inhibition of vascular endothelial growth factor activity by transfection with the soluble FLT-1 gene. J Cardiovasc Pharmacol 2000;36:498–502.
14. Clauss M, Weich H, Breier G, et al. The vascular endothelial growth factor receptor Flt-1 mediates biological activities. Implications for a functional role of placenta growth factor in monocyte activation and chemotaxis. J Biol Chem 1996;271:17629–34.
15. Heil M, Clauss M, Suzuki K, et al. Vascular endothelial growth factor (VEGF) stimulates monocyte migration through endothelial monolayers via increased integrin expression. Eur J Cell Biol 2000;79:850–7.
16. Sawano A, Iwai S, Sakurai Y, et al. Flt-1, vascular endothelial growth factor receptor 1, is a novel cell surface marker for the lineage of monocyte-macrophages in humans. Blood 2001;97:785–91.
17. Ishida A, Murray J, Saito Y, et al. Expression of vascular endothelial growth factor receptors in smooth muscle cells. J Cell Physiol 2001;188:359–68.

18. Fukushima K, Miyamoto S, Tsukimori K, et al. Tumor necrosis factor and vascular endothelial growth factor induce endothelial integrin repertories, regulating endovascular differentiation and apoptosis in a human extravillous trophoblast cell line. Biol Reprod 2005;73:172–9.

19. Forstreuter F, Lucius R, Mentlein R. Vascular endothelial growth factor induces chemotaxis and proliferation of microglial cells. J Neuroimmunol 2002;132:93–8.

20. Hiratsuka S, Maru Y, Okada A, Seiki M, Noda T, Shibuya M. Involvement of Flt-1 tyrosine kinase (vascular endothelial growth factor receptor-1) in pathological angiogenesis. Cancer Res 2001;61:1207–13.

21. Kaplan RN, Riba RD, Zacharoulis S, et al. VEGFR1-positive haematopoietic bone marrow progenitors initiate the pre-metastatic niche. Nature 2005;438:820–7.

22. Murakami M, Iwai S, Hiratsuka S, et al. Signaling of vascular endothelial growth factor receptor-1 tyrosine kinase promotes rheumatoid arthritis through activation of monocytes/macrophages. Blood 2006;108:1849–56.

23. Roggendorf W, Strupp S, Paulus W. Distribution and characterization of microglia/macrophages in human brain tumors. Acta Neuropathol (Berl) 1996;92:288–93.

24. Bettinger I, Thanos S, Paulus W. Microglia promote glioma migration. Acta Neuropathol (Berl) 2002;103:351–5.

25. Selvaraj SK, Giri RK, Perelman N, Johnson C, Malik P, Kalra VK. Mechanism of monocyte activation and expression of proinflammatory cytochemokines by placenta growth factor. Blood 2003;102:1515–24.

26. Machein MR, Renninger S, Lima-Hahn E, Plate KH. Minor contribution of bone marrow-derived endothelial progenitors to the vascularization of murine gliomas. Brain Pathol 2003;13:582–97.

27. Waltenberger J, Lange J, Kranz A. Vascular endothelial growth factor-A-induced chemotaxis of monocytes is attenuated in patients with diabetes mellitus: a potential predictor for the individual capacity to develop collaterals. Circulation 2000;102:185–90.

28. Brix G, Semmler W, Port R, Schad LR, Layer G, Lorenz WJ. Pharmacokinetic parameters in CNS Gd-DTPA enhanced MR imaging. J Comput Assist Tomogr 1991;15:621–8.

29. Grunewald M, Avraham I, Dor Y, et al. VEGF-induced adult neovascularization: recruitment, retention, and role of accessory cells. Cell 2006;124:175–89.

30. Harris AL. Hypoxia—a key regulatory factor in tumour growth. Nat Rev Cancer 2002;2:38–47.

31. Lewis CE, Pollard JW. Distinct role of macrophages in different tumor microenvironments. Cancer Res 2006;66:605–12.

32. Barbera-Guillem E, Nyhus JK, Wolford CC, Friece CR, Sampsel JW. Vascular endothelial growth factor secretion by tumor-infiltrating macrophages essentially supports tumor angiogenesis, and IgG immune complexes potentiate the process. Cancer Res 2002;62:7042–9.

33. Swift ME, Kleinman HK, DiPietro LA. Impaired wound repair and delayed angiogenesis in aged mice. Lab Invest 1999;79:1479–87.

34. Robinson-Smith TM, Isaacsohn I, Mercer CA, et al. Macrophages mediate inflammation-enhanced metastasis of ovarian tumors in mice. Cancer Res 2007;67:5708–16.

35. Goede V, Brogelli L, Ziche M, Augustin HG. Induction of inflammatory angiogenesis by monocyte chemoattractant protein-1. Int J Cancer 1999;82:765–70.

36. Adini A, Kornaga T, Firoozbakht F, Benjamin LE. Placental growth factor is a survival factor for tumor endothelial cells and macrophages. Cancer Res 2002;62:2749–52.

37. Luttun A, Tjwa M, Moons L, et al. Revascularization of ischemic tissues by PlGF treatment, and inhibition of tumor angiogenesis, arthritis and atherosclerosis by anti-Flt1. Nat Med 2002;8:831–40.

38. Das B, Yeger H, Tsuchida R, et al. A hypoxia-driven vascular endothelial growth factor/Flt1 autocrine loop interacts with hypoxia-inducible factor-1α through mitogen-activated protein kinase/extracellular signal-regulated kinase 1/2 pathway in neuroblastoma. Cancer Res 2005;65:7267–75.

39. Hattori K, Dias S, Heissig B, et al. Vascular endothelial growth factor and angiopoietin-1 stimulate postnatal hematopoiesis by recruitment of vasculogenic and hematopoietic stem cells. J Exp Med 2001;193:1005–14.

40. Hattori K, Heissig B, Wu Y, et al. Placental growth factor reconstitutes hematopoiesis by recruiting VEGFR1(+) stem cells from bone-marrow microenvironment. Nat Med 2002;8:841–9.

41. Pollard JW. Tumour-educated macrophages promote tumour progression and metastasis. Nat Rev Cancer 2004;4:71–8.

42. Marcellini M, De Luca N, Riccioni T, et al. Increased melanoma growth and metastasis spreading in mice overexpressing placenta growth factor. Am J Pathol 2006;169:643–54.

43. Carmeliet P, Moons L, Luttun A, et al. Synergism between vascular endothelial growth factor and placental growth factor contributes to angiogenesis and plasma extravasation in pathological conditions. Nat Med 2001;7:575–83.

44. Eriksson A, Cao R, Pawliuk R, et al. Placenta growth factor-1 antagonizes VEGF-induced angiogenesis and tumor growth by the formation of functionally inactive PlGF-1/VEGF heterodimers. Cancer Cell 2002;1:99–108.

45. Xu L, Cochran DM, Tong RT, et al. Placenta growth factor overexpression inhibits tumor growth, angiogenesis, and metastasis by depleting vascular endothelial growth factor homodimers in orthotopic mouse models. Cancer Res 2006;66:3971–7.

46. Oura H, Bertoncini J, Velasco P, Brown LF, Carmeliet P, Detmar M. A critical role of placental growth factor in the induction of inflammation and edema formation. Blood 2003;101:560–7.

47. Detmar M, Brown LF, Schon MP, et al. Increased microvascular density and enhanced leukocyte rolling and adhesion in the skin of VEGF transgenic mice. J Invest Dermatol 1998;111:1–6.

48. Luttun A, Brusselmans K, Fukao H, et al. Loss of placental growth factor protects mice against vascular permeability in pathological conditions. Biochem Biophys Res Commun 2002;295:428–34.

49. Odorisio T, Schietroma C, Zaccaria ML, et al. Mice overexpressing placenta growth factor exhibit increased vascularization and vessel permeability. J Cell Sci 2002;115:2559–67.